Infrared studies of ortho-para conversion at Cl-atom and H-atom impurity centers in cryogenic solid hydrogen

P.L. Raston*, S.C. Kettwich, and D.T. Anderson

Department of Chemistry, University of Wyoming, Laramie, WY 82071–3838, USA
E-mail: danderso@uwyo.edu

We report infrared spectroscopic studies of H_2 ortho-para (o/p) conversion in solid hydrogen doped with Cl-atoms at 2 K while the $Cl + H_2(v = 1) \rightarrow HCl + H$ infrared-induced chemical reaction is occurring. The Cl-atom doped hydrogen crystals are synthesized using 355 nm *in situ* photodissociation of Cl_2 precursor molecules. For hydrogen solids with high ortho-H_2 fractional concentrations ($X_o = 0.55$), the o/p conversion kinetics is dominated by Cl-atom catalyzed conversion with a catalyzed conversion rate constant $K_{cc} = 1.16(11)$ min^{-1} and the process is rate-limited by ortho-H_2 quantum diffusion. For hydrogen crystals with low ortho-H_2 concentrations ($X_o = 0.03$), single-exponential decay of the ortho-H_2 concentration with time is observed which is attributed to H-atom catalyzed o/p conversion by the H-atoms produced during the infrared-induced $Cl + H_2$ reaction. The measured H-atom catalyzed o/p conversion kinetics indicates the H-atoms are mobile under these conditions in agreement with previous ESR measurements.

1. Introduction

The study of chemical reactions carried out in solid hydrogen crystals at liquid helium temperatures allow for a variety of low-temperature quantum phenomena to be explored under very controlled conditions [1,2]. Our group has been studying the details of the infrared-induced chemical reaction, $Cl(^2P_{3/2}) + H_2(v = 1) \rightarrow HCl + H$, in highly enriched (99.99%) parahydrogen (pH_2) crystals at temperatures around 2 K [2–5]. This prototypical hydrogen abstraction reaction proceeds at these low temperatures via vibrational excitation of the H_2 reagent since the reaction of Cl with $H_2(v = 0)$ has a ~1900 cm^{-1} barrier and is $+ 360$ cm^{-1} endothermic [6–8]. To better understand the photochemical mechanism by which infrared (IR) light creates $H_2(v = 1)$ and triggers the $Cl + H_2$ reaction, we studied the IR-induced reaction kinetics as a function of the orthohydrogen (oH_2) concentration in the solid. This led us to wonder about the effects of ortho-para (o/p) conversion caused by the Cl-atom reagent and H-atom product. Specifically, we need to measure to what extent

the oH_2 concentration changes during the course of the IR-driven reaction to test if we can measure the reaction kinetics at a fixed oH_2 concentration.

The fractional oH_2 concentration (X_o) of solid hydrogen can be measured using Fourier transform infrared spectroscopy (FTIR) via the intensities of specific solid hydrogen absorptions that are proportional to the oH_2 and pH_2 content. For example, recently Abouaf-Marguin and coworkers [9] established an empirical law to determine X_o using FTIR spectroscopy to study o/p conversion in solid normal hydrogen (nH_2) doped with O_2 molecules. These studies show that the paramagnetic O_2 impurity catalyzes o/p conversion within the solid at 4.2 K. The heavy O_2 impurity is immobile in solid hydrogen at these temperatures and thus the kinetics of o/p conversion is diffusion controlled and limited by the rate at which oH_2 diffuses next to an O_2 molecule within the solid. Our expectation is that the Cl-atom radical should behave similar to O_2 since it too should be immobile under our conditions. The effects of Cl-atom catalyzed o/p conversion should only be impor-

tant at relatively high initial oH_2 concentrations ($X_o \geq 0.1$), since the Cl-atom concentration is very low (on the order of 100 parts-per-million) under the conditions that the IR-induced reaction is studied.

The o/p conversion kinetics in solid hydrogen catalyzed by the H-atom product, however, should be qualitatively different because the H-atom is mobile even at temperatures below 2 K. It is well known that H-atoms diffuse in solid hydrogen by quantum mechanical tunneling at temperatures below 4 K [10–15]. The most recent ESR measurements from the group at Nagoya University indicate the H-atoms translate via «chemical diffusion» whereby the H-atom moves by the $H + H_2 \rightarrow H_2 + H$ chemical reaction between an H-atom and one of its surrounding H_2 molecules in the solid [14]. Through a variety of ESR measurements, the Nagoya group examined both H-atom diffusion and recombination separately as a function of the oH_2 concentration in the crystal at ~4 K [13]. These measurements show that at $X_o \geq 0.1$ the recombination rate is consistent with the measured diffusion rate, while at $X_o < 0.1$ the recombination rate is too slow to be explained by the diffusion rate [13]. This suggests that at low X_o the diffusion rate is still significant but the H-atoms do not recombine due to the details of chemical diffusion in relatively pure pH_2.

The purpose of this study is to measure the effects of Cl-atom and H-atom catalyzed o/p conversion during the course of the IR-induced $Cl + H_2$ chemical reaction in solid hydrogen at $X_o = 0.03$ and 0.5 and at temperatures around 2 K. The measured Cl-atom catalyzed o/p conversion kinetics should be similar in many respects to recent FTIR studies of o/p conversion in O_2 doped solid nH_2 [9]. This is the first time to our knowledge, however, that FTIR measurements have been used to follow H-atom catalyzed o/p conversion in solid hydrogen.

The measurements presented here compliment previous ESR measurements [10–15] of H-atom diffusion in solid hydrogen because the kinetics of o/p conversion depends on the H-atom diffusion rate. These FTIR measurements are also comparable to older gas-chromatography measurements [11] which measured X_o in hydrogen solids before and after exposure to H-atoms, but in this case, we can follow the o/p conversion kinetics directly and nondestructively.

This paper is organized as follows. In the next section we describe the experimental techniques used to synthesize and characterize the Cl-atom doped hydrogen crystals. We report the Cl-atom quantum yield for 355 nm photolysis of Cl_2 in solid pH_2 in Sec. 3 along with FTIR measurements of the Cl-atom concentration and X_o. In Sec. 3 we present measurements of the time-dependence of the Cl-atom concentration during the IR-induced reaction which are, in turn, used to interpret the measured o/p conversion kinetics for crystals with $X_o = 0.03$ and 0.5. Finally, in Sec. 4 we summarize our main results.

2. Experimental

We use the «rapid vapor deposition» technique developed by Fajardo and Tam to produce ~2 mm thick optically transparent crystals of Cl_2 doped solid hydrogen [16,17]. The Cl_2 doped hydrogen crystals are grown by co-deposition of two separate gas streams, the H_2 host (Linde Gas, purity: 99.999%) and Cl_2 dopant (Aldrich, purity: 99.5%), onto a BaF_2 optical substrate cooled to ~2.5 K within a liquid He bath cryostat. The oH_2 content in the crystal is varied by passing nH_2 gas through a variable low-temperature o/p converter just prior to deposition. Since o/p conversion within solid hydrogen is very slow [18], the oH_2 concentration in the solid is dictated by the thermal equilibrium established in the o/p converter. The oH_2 concentration in the crystal can be predicted, therefore, from the temperature of the o/p converter ($T_{o/p}$) using the rotational partition function of H_2 and assuming complete equilibration. When the o/p converter is operated at either 30 or 80 K, the corresponding X_o values are, respectively, 0.0295 and 0.514. The oH_2 concentration of the crystal can also be measured spectroscopically and the two IR-based methods used here will be described in Sec. 3. The IR pathlength through the crystal is determined using the integrated intensities of the $Q_1(0) + S_0(0)$ and/or the $S_1(0) + S_0(0)$ solid hydrogen double transitions and the proportionality constants 90(2) cm^{-2} and 7.0(2) cm^{-2}, respectively, determined by Fajardo [19]. We use the term «as-deposited» to refer to hydrogen crystals right after rapid vapor deposition which have never been exposed to temperatures above ~2.5 K. The as-deposited crystals are known to exhibit a mixed hexagonal-close-packed and face-centered-cubic crystalline morphology [16,20].

The Cl-atom doped pH_2 solids are prepared by 355 nm *in situ* UV photolysis of the Cl_2 precursor molecule [3,4]. The Cl_2 doped pH_2 crystals are photolyzed using the third harmonic (355 nm) of a Nd:YAG laser operating at 10 Hz with a pulse energy of 2 mJ/pulse and cross sectional area of ~50 mm^2, which impinges on the solid at 45° with respect to the substrate surface normal. All UV photolysis experiments are carried out on as-deposited samples at temperatures ~2 K.

IR spectra are recorded with a FTIR spectrometer (Bruker IFS 120-HR) using a transmission optical setup where the IR beam is focused through the sample with the main optical axis parallel to the substrate surface normal. Mid-IR spectra at 0.1 cm^{-1} resolution from 800 to 3800 cm^{-1} are recorded with the FTIR equipped with a KBr beamsplitter, a globar source filtered with a 3861 cm^{-1} long pass filter (LPF), and MCT detector. Near-IR spectra from 2000 to 8000 cm^{-1} at 0.1 cm^{-1} resolution are recorded using a CaF_2 beamsplitter, a tungsten source, and InSb detector. Experiments measuring the IR-induced $Cl + H_2$ reaction and o/p conversion kinetics are carried out using the near-IR FTIR setup with 127 s acquisition times (16 scans at

0.1 cm^{-1} resolution). Care was taken during UV photolysis to insure that no IR light > 4000 cm^{-1} impinged on the sample to prevent IR-induced chemical reactions [3].

3. Experimental results and discussion

3.1. 355 nm Cl-atom quantum yield and Cl spin–orbit transition strength

Figure 1,*a* displays IR spectra in the region of the zero-phonon Cl spin–orbit (SO) transition for a 120 parts-per-million Cl$_2$ doped pH$_2$ crystal ($X_o \leq 0.0003$) as a function of exposure to the 355 nm photolysis laser. The mid-IR spectra are recorded with the 3861 cm^{-1} LPF in the FTIR beam to insure that no IR-induced photochemistry occurs while recording the spectra [3]. The bottom trace was recorded before UV photolysis for the Cl$_2$ doped as-deposited sample and shows no detectable absorption feature in this region. Subsequent traces, displaced upward with increasing exposure to the UV phololysis laser, show growth in the integrated intensity of the Cl SO transition at 943.8 cm^{-1} [4]. The upper most trace is for a total of 560 s of exposure to the 355 nm photolysis laser. The 355 nm photoproduction of isolated Cl-atoms is consistent with previous reports [3–5] from this laboratory for photolysis of Cl$_2$ in solid pH$_2$ carried out in the absence of IR light at energies above 4000 cm^{-1}.

Using the data shown in Fig. 1,*a*, a growth curve for the *in situ* 355 nm photoproduction of Cl in solid pH$_2$ is plotted in Fig. 1,*b*. The Cl-atom growth rate is found to be approximately first-order. The quantum yield (Φ) for the photoproduction of Cl is determined using the following first-order exponential growth expression [21,22]:
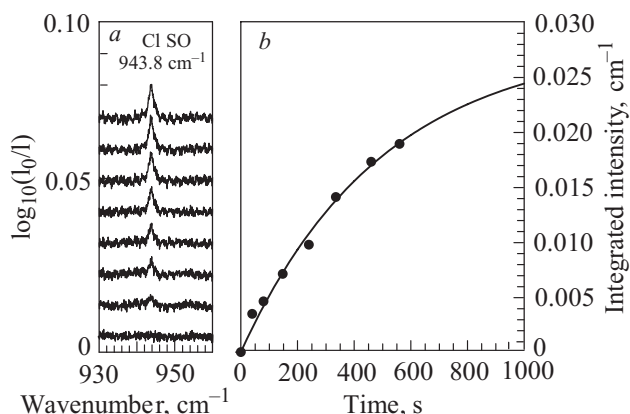
$$I(t)=I(t=\infty)\,[1-\exp\,(-\sigma I_{355}\Phi t)]\,, \qquad (1)$$

where $I(t)$ and $I(t=\infty)$ are the integrated intensities of the Cl SO transition at photolysis time t and $t=\infty$, respectively, σ is the gas-phase cross section [23] of Cl$_2$ at 355 nm $(16.2\cdot10^{-20}$ cm^2), and I_{355} is the laser fluence $(7.11\cdot10^{16}$ photons/cm$^2\cdot$s) used in the experiment. Using these values, the quantum yield for the production of Cl is found to be $\Phi = 0.17(3)$, where the reported error is the uncertainty (1σ) in Φ determined from the least-squares fit of the data to Eq. (1). This value differs slightly from the previously reported [5] value ($\Phi = 0.3$) due to re-analysis of the integrated intensities of the Cl SO transition. The error in the reported quantum yield is likely larger due to the weak transition strength for the Cl SO transition which makes it difficult to determine accurate integrated intensities.

While the reported 355 nm Cl-atom quantum yield is small, it is still large enough so that 355 nm *in situ* photo-dissociation of Cl$_2$ can be used to produce Cl-atom doped solid pH$_2$. We view these measurements as providing two important pieces of information. First, the quantum yield is not zero whereas for many condensed phase photodissociation reactions of relatively heavy atoms (e.g., Cl) the quantum yield is extremely small due to the «cage effect» of the solvent which keeps the nascent photofragments in close proximity [21,22]. Second, the extracted photolysis rate constant ($k = \sigma I_{355}\Phi$) allows us to design experimental conditions such that we can be assured that most of the Cl$_2$ has been photodissociated prior to any IR-induced photochemistry. Under the present experimental conditions, the Cl-atom photoproduction rate ($k = 2.0(4)\cdot10^{-3}$ s^{-1}) suggests the Cl$_2$ molecule has a half-live of 347 s and so by carrying out the photolysis for several half-lives, most (if not all) of the Cl$_2$ is photodissociated before we start to study the IR-induced chemistry.

The Cl SO transition is electric dipole-forbidden in the gas phase and thus has a weak transition strength of $S = 9.45\cdot10^{-21}$ cm/mol [24]. To measure the Cl SO transition strength for a Cl-atom solvated in solid pH$_2$, we again used the data in Fig. 1. We calculated the Cl-atom concentration at each step in the photolysis using the initial Cl$_2$ concentration and assuming the photolysis rate followed Eq. (1). To convert ppm factional concentrations to molecules per cm^3 we used the number density of solid pH$_2$ at liquid helium temperatures $(2.600\cdot10^{22}$ mol/cm^3) [18,25]. We then made a plot of integrated intensity divided by pathlength ($l = 0.33$ cm) as a function of Cl-atom concentration and fit the data to a straight line with the origin fixed at zero. This analysis showed $S = 3.1(1)\cdot10^{-20}$ cm/mol, where the error only reflects errors from the least-squares fit. This analysis is consistent with previous estimates and confirms that solvation in solid pH$_2$ only slightly increases the Cl SO transition strength (about a factor of 3). The largest uncertainty in

Fig. 1. Infrared spectroscopic data used to determine the Cl-atom quantum yield (Φ) for the 355 nm photolysis of Cl$_2$ in solid pH$_2$. (*a*) A series of IR spectra of the Cl SO transition displaced upward with increasing exposure times to the 355 nm photolysis laser. (*b*) Plot of the Cl SO integrated intensity (black circles) versus photolysis time at 1.95 K. The solid line is a fit of Eq. (1) to the data used to determine Φ.

this procedure is in the determination of the Cl-atom concentration which is calculated based on the Cl_2 and H_2 gas flow rates during deposition.

3.2. Monitoring the Cl-atom concentration in the near-IR

To study the kinetics of o/p conversion while the IR-induced $Cl + H_2$ reaction is occurring, it is necessary to monitor the Cl-atom concentration as a function of time since the Cl-atom is paramagnetic and thus a potential o/p catalyst. As discussed above, the Cl-atom concentration can be monitored by measuring the integrated intensity of the Cl SO transition. However, the intensity of this transition is quite weak. The Cl SO + $S_0(0)$ double transition, which arises from simultaneous SO excitation of the Cl-atom and rotational ($J = 2 \leftarrow 0$) excitation of a neighboring pH_2 molecule, is approximately 4 times more intense than the zero-phonon Cl SO transition [4]. Unfortunately, the Cl SO + $S_0(0)$ double transition is relatively broad (~ 25 cm^{-1}) making the peak intensity low and thus this transition is also not very useful for monitoring the Cl-atom concentration at ~ 100 ppm levels.

Fortunately the Cl SO + $Q_1(0)$ double transition is relatively sharp and intense making it well suited for monitoring the Cl-atom concentration under these conditions. Figure 2 shows the near-IR difference spectrum generated from spectra recorded before and after 20 min of 355 nm UV photolysis of a 2.0(1) mm thick Cl_2-doped pH_2 sample with an initial Cl_2 concentration of ~ 50 ppm and $X_o = 0.0003$. This feature is easily assigned to the Cl SO + $Q_1(0)$ double transition because the peak transition energy at 5094.72 cm^{-1} is 4150.9 cm^{-1} higher than the Cl SO transition (943.8 cm^{-1}), and this difference corresponds almost quantitatively to the known $Q_1(0)$ vibron band energy (4153 cm^{-1}) in solid pH_2 [26]. Further, the Cl SO +

$+ S_1(0)$ double transition is also observed at 5426.16 cm^{-1}, which is 4482.4 cm^{-1} higher in energy than the Cl SO transition that also compares well to the $S_1(0)$ transition frequency in solid pH_2 (4486.1 cm^{-1}) [27].

Using the integrated intensity of the Cl SO + $Q_1(0)$ transition from five separate crystals, the measured thicknesses of the crystals, and assuming the 355 nm Cl_2 photodissociation follows Eq. (1) with the initial Cl_2 concentration determined from gas flow rates, the integrated intensity of the Cl SO + $Q_1(0)$ double transition is estimated to be $2.3(2) \cdot 10^{-19}$ cm/mol which is approximately a factor of 7 stronger than the intensity of the Cl SO transition. Therefore, in the following kinetic studies we will use the Cl SO + $Q_1(0)$ double transition to monitor the Cl-atom concentration. The only drawback to using the intensity of this absorption feature to monitor the Cl-atom concentration is that since the Cl SO + $Q_1(0)$ transition energy is greater than 4000 cm^{-1}, the IR-radiation from the FTIR source used to record the spectra of this feature causes the Cl-atom to react with the pH_2 solid via the reaction $Cl + H_2(v = 1) \rightarrow HCl + H$ [3]. However, the IR-induced reaction rate is still slow compared to the acquisition time of the FTIR spectra (approximately 127 s) such that the kinetics of the Cl-atom decay caused by the IR-induced reaction can be followed using this transition.

3.3. Monitoring the oH_2 concentration

The X_o value in a given crystal can be measured using the integrated intensities of specific solid hydrogen IR transitions. In this work we will utilize two methods depending on the initial X_o value in the crystal. At relatively high oH_2 concentrations ($X_o \geq 0.5$), we will use the empirical formula developed by Abouaf-Marguin and Vasserot [9] that utilizes the intensity of the solid hydrogen double transitions at 4505 and 4736 cm^{-1}. The IR spectrum of a Cl-atom doped H_2 solid with approximately $X_o = 0.5$ is shown in Fig. 3. The intensities of the two double transitions used in this analysis, labeled $I(4505)$ and $I(4736)$ in Fig. 3, are proportional to the pH_2 and oH_2 concentrations, respectively. Spectra are integrated from 4478 to 4520.5 cm^{-1} to determine $I(4505)$ and from 4719 to 4763 cm^{-1} to determine $I(4736)$ and the integration limits and baselines are indicated by the dotted lines in Fig. 3. These intensities are then used in the following equation [9]:

$$\frac{N_o}{N_p} = \frac{1}{0.565} \frac{I(4736)}{[I(4505) - 0.11\, I(4736)]}, \quad (2)$$

where the factor 0.565 accounts for the different transition strengths of $I(4505)$ and $I(4736)$ and the factor 0.11 takes into account a small oH_2 contribution to the $I(4505)$ pH_2 peak. Using this equation we calculate $X_o = 0.5479(2)$ and 0.5497(2) for two separate samples that were deposited with $T_{o/p} = 80$ K corresponding to $X_o = 0.5137$. This ana-
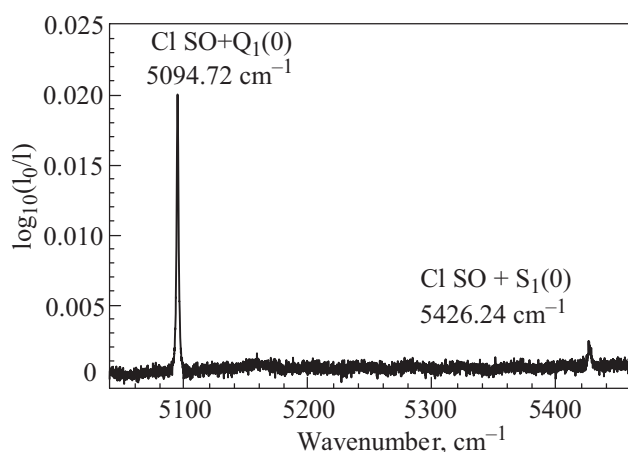

Fig. 2. Difference spectrum showing the Cl SO + $Q_1(0)$ and Cl SO + $S_1(0)$ double transitions resulting from the 355 nm photolysis of a Cl_2 doped pH_2 solid. The Cl SO + $Q_1(0)$ transition is used to monitor the Cl-atom concentration as a function of time.
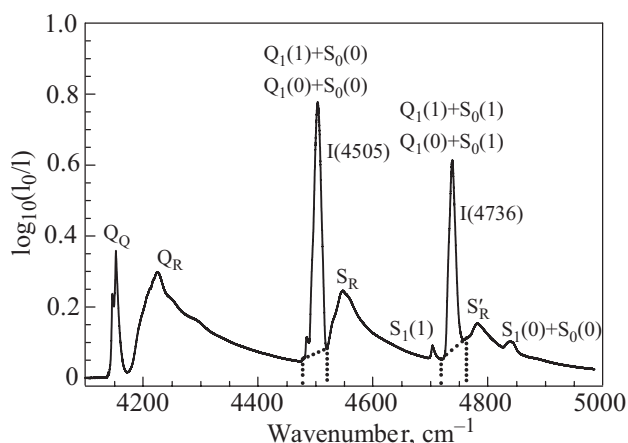
Fig. 3. Near-IR spectrum in the region of the fundamental solid hydrogen transitions for a Cl_2 doped hydrogen solid with $X_o \approx 0.55$ recorded at 2.14 K right after 15 min of 355 nm photolysis. The dotted line segments indicate baselines and integration limits used to determine $I(4505)$ and $I(4736)$ in order to spectroscopically measure X_o for samples with high initial oH_2 content.
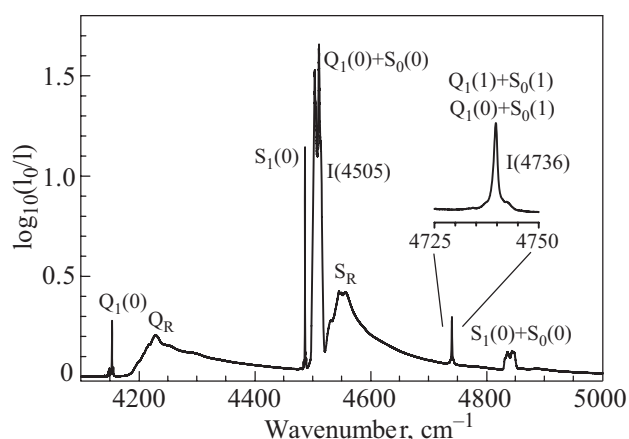

Fig. 4. Near-IR spectrum in the region of the fundamental solid hydrogen transitions for a Cl_2 doped pH_2 sample with $X_o \approx 0.03$ recorded at 1.93 K right after 20 min of 355 nm photolysis. The inset shows the two overlapping double transitions (i.e., $Q_1(1) + S_0(1)$ and $Q_1(0) + S_0(1)$) used under these lower oH_2 concentration conditions to spectroscopically measure X_o as a function of time.

lysis suggests the absolute X_o values are good to within 10%.

At X_o values less than 0.05, the $I(4505)$ pH_2 feature typically has a maximum absorption ($A = \log_{10}(I_0/I)$) above 1.0 (for approximately 2 mm thick samples) and thus the method described above to spectroscopically monitor X_o was found to produce significant scatter in the measured value. For samples in this oH_2 concentration range ($X_o \leq 0.05$) we simply integrate the $I(4736)$ double transition with narrower integration limits (4727 to 4750 cm^{-1}) to reduce the noise in the intensity measurement. The IR spectrum of a Cl-atom doped pH_2 solid with $X_o \approx 0.03$ is shown in Fig. 4. Comparison of the $I(4736)$ feature in Figs. 3 and 4 shows that at lower oH_2 concentrations this feature is significantly sharper and thus more precise measurements of X_o are possible. The transition strength for $I(4736)$ was determined using the oH_2 concentration calculated from the temperature of the o/p converter ($T_{o/p} = 30$ K and $X_o = 0.02947$) and the measured thickness of the sample. The $I(4736)$ transition strength is therefore estimated to be $6.47(4) \cdot 10^{-21}$ cm/mol. We can independently measure the X_o value using the integrated intensity of the $Q_1(0)$ transition from 4151 to 4154 cm^{-1} and the proportionality constant reported by Tam and Fajardo [17], which leads to $X_o = 0.0269(5)$. Based on this analysis, for X_o values determined using just $I(4736)$ for crystals with $X_o \leq 0.05$, the reported X_o value is likely good to within 10%, similar to the errors for the method of Abouaf-Marguin and Vasserot [9]. Note using Eq. (1) from Tam and Fajardo [17] the proportionality constant b for the $I(4736)$ feature is predicted to be 73 cm^{-2} (with $\tilde{v}$ in cm^{-1} and l in cm).

3.4. Cl-*atom decay profiles in solid* H_2 *with* $X_o \approx 0.55$ *and* 0.03

As discussed previously, the IR radiation from the FTIR spectrometer used to measure the Cl SO + $Q_1(0)$ transition induces the Cl + $H_2(v = 1) \rightarrow$ HCl + H reaction and thus the Cl-atom concentration decays with time when IR light at energies > 4000 cm^{-1} irradiates the crystal [2,3]. In order to quantify to what extent the Cl-atom catalyzes o/p conversion within the solid, we need to know the time profile of the Cl-atom concentration. In Fig. 5 we plot the
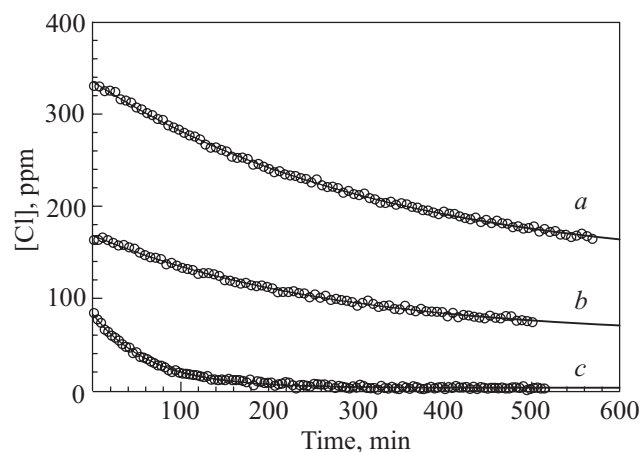

Fig. 5. Decay of the Cl-atom concentration with time for three different H_2 crystals exposed to near-IR radiation. The H_2 crystal conditions are as follows: $[Cl_2] = 185$ ppm, $X_o = 0.55$, 2.13 K (*a*), $[Cl_2] = 130$ ppm, $X_o = 0.55$, 2.13 K (*b*), and $[Cl_2] = 50$ ppm, $X_o = 0.03$, 1.93 K (*c*). The solid lines are fits of Eq. (3) to the data. Note the Cl-atom concentration does not decay fully in the samples with high initial X_o values.

Cl-atom concentration as a function of IR exposure time for three separate Cl-atom doped H_2 crystals. The basic procedure used to record these time profiles are the same for all three samples. First a Cl_2 doped H_2 solid is deposited and then photolyzed with 355 nm UV radiation for a set amount of time (15 to 20 min) to produce the Cl-atom doped sample. After UV photolysis is complete, the sample is exposed to IR radiation from the FTIR source that contains IR photons at energies greater than 4000 cm^{-1} and repeated near-IR spectra are recorded for approximately 8 h. The IR irradiation time is limited by the hold time of the liquid helium cryostat. Typically, spectra are recorded at 4 min intervals with 127 s acquisition times at a spectral resolution of 0.1 cm^{-1}. The integrated intensity of the Cl SO + $Q_1(0)$ transition measured in these spectra are used to calculate the Cl-atom concentration in ppm to generate the data shown in Fig. 5.

The three traces in Fig. 5 are for two samples with high X_o (labeled *a* and *b*) and one with low X_o (labeled *c*). As will be discussed in a separate publication [28], the kinetics of the IR-induced Cl + H_2 reaction depends on the oH_2 concentration in the crystal. At high X_o values ($X_o = 0.55$) the reaction slows down and does not go to completion. All three data sets in Fig. 5 are well fit by a simple exponential function,

$$[Cl] = [Cl]_\infty + A \exp\left(-kt\right), \qquad (3)$$

where $[Cl]_\infty$ is the Cl-atom concentration at infinite reaction time, A is the magnitude of the $[Cl]$ decrease, and t is the total time of IR exposure. The fitted parameters are given in Table 1. The IR-induced reaction rate constant is larger for crystals with lower X_o values. In addition, at high X_o values the reaction does not proceed to completion, which can be seen by the $[Cl]_\infty$ values reported in Table 1 for crystals (a) and (b) which remain at 35–40% of the initial Cl concentration even after prolonged IR exposure. The implications of this oH_2 concentration effect on the IR induced reaction kinetics are beyond the scope of this paper, but the details of these Cl-atom concentration profiles will be used to interpret the o/p conversion kinetic data.

Table 1. Fitted parameters determined from least-squares fits of Eq. (3) to the Cl-atom concentration data during IR exposure for four separate crystals

Crystal	X_o	$[Cl]_\infty$, ppm	A, ppm	k, min^{-1}
a	0.55	132(2)	204(1)	$3.05(5) \cdot 10^{-3}$
b	0.55	59(2)	110(1)	$3.64(12) \cdot 10^{-3}$
c	0.03	3.4(2)	79.5(7)	$15.4(2) \cdot 10^{-3}$
d	0.03	7.1(6)	132(1)	$10.0(2) \cdot 10^{-3}$

3.5. Cl-*atom catalyzed o/p conversion in* $X_o \approx 0.55$ *hydrogen solids*

The first evidence of Cl-atom catalyzed o/p conversion was provided by lineshape analysis of the Cl SO + $Q_1(0)$ transition in H_2 crystals with high X_o values. Selected IR spectra during the course of the IR-induced reaction are shown in Fig. 6 for crystal (a). The spectra in Fig. 6 are displaced downward with increasing IR exposure time. The Cl SO + $Q_1(0)$ transition energy (5094.72 cm^{-1}) measured for a low $X_o = 0.0003$ pH_2 solid is indicated in Fig. 6 by a dashed line. Careful examination of the Cl SO + $Q_1(0)$ lineshape at this high initial oH_2 concentration ($X_o \approx 0.55$) shows that the peak transition energy and FWHM change during the early stages of the IR-driven reaction. Shown in Fig. 7 are plots of the FWHM (cm^{-1}) and peak shift (cm^{-1}) as a function of the IR exposure time. The peak shift is defined here as the measured peak position minus the Cl SO + $Q_1(0)$ transition energy measured for low X_o pH_2 solids, namely *peak shift* = ν_{max} — 5094.72 cm^{-1}. Both data sets are well-fit by a double exponential equation

$$Y(t) = y_0 + A\left[1 - \exp\left(-at\right)\right] + B\left[1 - \exp\left(-bt\right)\right]. \qquad (4)$$

The results of least-squares fits of the FWHM and peak shift data to Eq. (4) are presented in Table 2. The Cl SO + $Q_1(0)$ peak shifts to lower energy (0.59 cm^{-1}) and narrows (0.94 cm^{-1}) during the ~500 min IR exposure. We interpret this as proof that the paramagnetic Cl-atom converts nearby oH_2 molecules with the faster rate constants extracted from the fits. The peak shift changes faster than the FWHM because the observed peak transition energy is heavily weighted by nearest-neighbor interactions, while
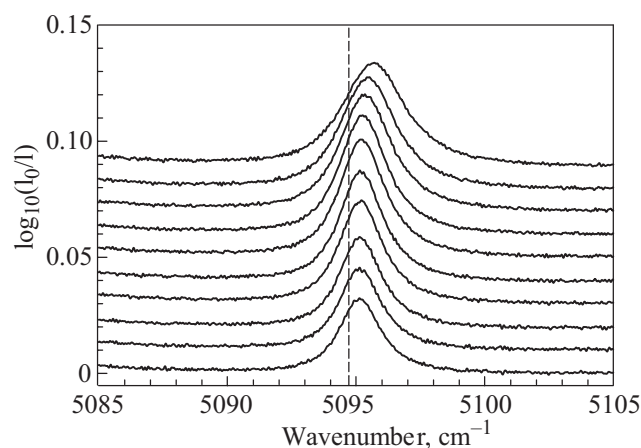

Fig. 6. A series of spectra of the Cl SO + $Q_1(0)$ transition illustrating the time dependence of this feature for a sample with an initial $X_o = 0.55$. The IR spectra are displaced downward with increasing IR exposure time showing that the feature sharpens and shifts toward lower frequency while constantly decaying in intensity. The dashed line indicates the Cl SO + $Q_1(0)$ transition frequency measured for Cl in highly enriched pH_2 solids ($X_o = 0.0003$).
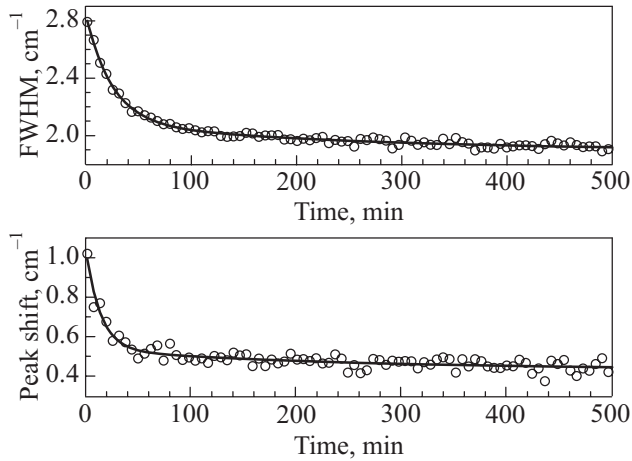
Fig. 7. Plots of the Cl SO + $Q_1(0)$ FWHM and peak shift data (open circles) as a function of IR exposure time for the spectra shown in Fig. 6. The solid lines are fits of Eq. (4) to the data.

Fig. 8. Plots of X_o as a function of IR exposure time for two different Cl-atom doped solid hydrogen samples with initial $X_o \approx 0.55$ values. The data for 170 ppm (squares) and 340 ppm (circles) initial Cl-atom concentrations show that o/p conversion rate speeds up at the higher Cl-atom concentrations. The dashed lines indicate the oH$_2$ self-conversion rate (without catalyst) for samples with these initial oH$_2$ concentrations. The solid lines are the results of fits of Eq. (5) to the data.

the FWHM is more sensitive to long-range interactions. After the Cl-atom converts all the oH$_2$ molecules within some critical distance, then on a longer timescale and with a slower rate constant, oH$_2$ molecules diffuse to the Cl-atom and get converted, such that the bulk concentration of oH$_2$ decays with the slower rate constant extracted from the fits. Indeed, the slower rate constant ($4.2 \cdot 10^{-3}$ min^{-1}) measured here is in the range of the rate constants (5–12$\cdot 10^{-3}$ min^{-1}) measured for the formation of oH$_2$ dimers in almost pure pH$_2$ solids which is a measure of the oH$_2$ quantum diffusion rate [29]. Once the Cl-atom is generated photolytically, it converts all the oH$_2$ molecules that are nearby with a fast rate and then once these oH$_2$ molecules are depleted, the o/p conversion process becomes rate-limited by the oH$_2$ quantum diffusion rate to the Cl-atom reaction center. Since the Cl-atoms are preset at low concentration, the initial fast local o/p conversion does not change the bulk X_o value very much. However, oH$_2$ quantum diffusion to the Cl-atoms that occurs on the slower timescale is the mechanism by which the bulk X_o value changes with time. It is therefore useful to measure the time dependence of X_o using solid hydrogen double transitions instead of the Cl SO + $Q_1(0)$ transition.

Table 2. Fitted parameters determined from least-squares fits of Eq. (4) to the FWHM and peak shift data for the Cl SO + $Q_1(0)$ transition during IR exposure for a crystal with $X_o \approx 0.55$

Data	y_0, cm^{-1}	A, cm^{-1}	a, min^{-1}	B, cm^{-1}	b, min^{-1}
FWHM	1.89(1)	0.74(2)	$4.0(3) \cdot 10^{-2}$	0.20(2)	$4.2(11) \cdot 10^{-3}$
Peak shift	0.43(2)	0.49(4)	$7.1(11) \cdot 10^{-2}$	0.10(2)	$4.2(28) \cdot 10^{-3}$

The bulk oH$_2$ concentration for the two crystals with initial $X_o \approx 0.55$ values are plotted in Fig. 8 as a function of IR exposure time. In both cases X_o decreases with time and
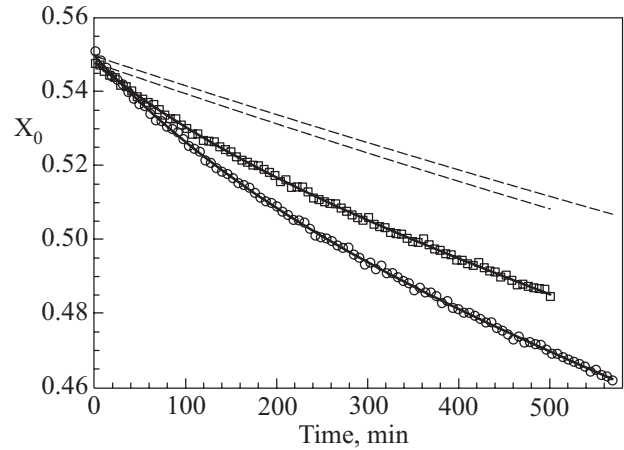
with a faster rate for the sample with the higher Cl-atom concentration. The o/p conversion rate in pure hydrogen solids is known to be second-order with respect to X_o [18] and has a self-conversion rate constant of $K_{sc} = 1.90(5)$%/h [18]. The self-conversion rate is second-order with respect to X_o because only the total nuclear spin $I = 1$ oH$_2$ species generates inhomogeneous magnetic fields that can induce o/p conversion, the $I = 0$ pH$_2$ molecule cannot. The change in X_o with time calculated using the self-conversion rate with slightly different initial oH$_2$ concentrations for both crystals are shown as dashed lines in Fig. 8. Clearly the measured decay in X_o is significantly greater than the predicted self-conversion rate indicating that the Cl-atoms catalyze the o/p conversion. The X_o data are well fit by an expression developed for catalyzed conversion by O$_2$ molecules [30], namely

$$\frac{1}{C(t)} = \frac{1}{C(0)} \exp(bt) + \frac{K_{sc}}{b} [\exp(bt) - 1], \qquad (5)$$

where $b \equiv K_{cc} C_p$, K_{sc} is the self-conversion rate constant, K_{cc} is the catalyzed conversion rate constant, $C(0)$ is the X_o value at $t = 0$, and C_p is the concentration of the catalyst species, in this case the Cl-atom. Since the catalyst concentration is time-dependent, we fit Eq. (5) to the data using the $C_p(t)$ profiles calculated from the data in Fig. 5. The results of the fit are shown as solid lines in Fig. 8 and the fitted parameters are presented in Table 3. The average self-conversion rate constant (1.62(5) %/h) extracted from the fits agrees well with the literature value (1.90(5) %/h) [18]. The average catalyzed conversion rate constant

(1.16(11) min^{-1}) for a Cl-atom is significantly larger than the value measured for O_2 catalysis, $K_{cc} = 0.17(3)$ min^{-1} [9]. This might be due to contributions from H-atom catalyzed o/p conversion. However, the fact that the data are well fit by Eq. (5) which uses the Cl-atom concentration for $C_p(t)$ supports the interpretation that Cl-atoms are catalyzing o/p conversion under these conditions.

Table 3. Fitted parameters determined from least-squares fits of Eq. (5) to X_o data during IR exposure for two crystals with initial $X_o \approx 0.55$ values

Crystal	C_0	K_{sc}, min^{-1}	K_{cc}, min^{-1}
a	0.5497(2)	$2.56(9) \cdot 10^{-4}$	1.05(3)
b	0.5479(2)	$2.83(8) \cdot 10^{-4}$	1.26(5)

3.6. H-*atom catalyzed o/p conversion in* $X_o \approx 0.03$ *hydrogen solids*

The next step is to analyze the o/p conversion data for highly enriched pH_2 solids ($X_o = 0.03$). First, the perturbation of the Cl $SO + Q_1(0)$ transition observed for the crystals with nominally $X_o = 0.0295$ values is very small. The Cl $SO + Q_1(0)$ lineshape is not at significantly higher transition energies and/or broader compared to the absorption feature measured for a crystal with $X_o = 0.0003$. Shown in Fig. 9 is a plot of X_o with time (open circles) measured for crystal (c) with an initial $X_o = 0.02916$ value. Attempts to fit this data to Eq. (5) failed and if the parameters reported in Table 3 for K_{cc} are used with the Cl-atom time profile and initial X_o value for this crystal, the predicted X_o time dependence is shown by the dashed line in Fig. 9. Under these conditions, since the Cl-atom
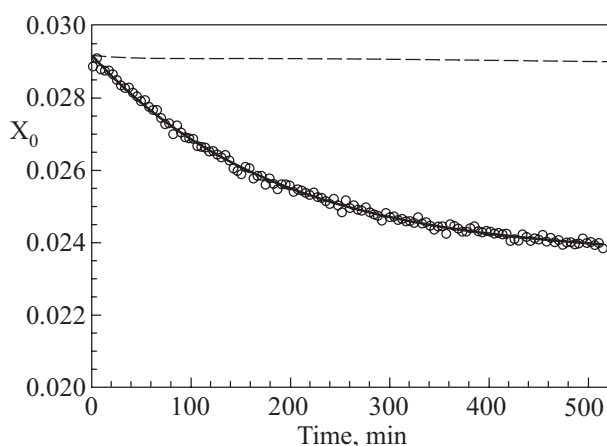

Fig. 9. Plots of X_o as a function of the IR exposure time for a Cl-atom doped pH_2 sample with an initial $X_o \approx 0.0292$ value. The X_o data is well fit by single-exponential decay as shown by the solid line. The dashed line indicates the predicted X_o time dependence for Cl-atom catalyzed conversion. The large disparity between the dashed and solid lines is taken as evidence for H-atom catalyzed o/p conversion.

concentration quickly decays in the first 100 min (see Fig. 5), there is no way to account for the large amount of o/p conversion that is observed based solely on Cl-atom o/p catalysis. Indeed for highly enriched pH_2 crystals it appears that a qualitatively different mechanism is dominant.

As the Cl-atom concentration decays in time via the IR-induced Cl + $H_2(v = 1) \rightarrow$ HCl + H chemical reaction, H-atoms are produced. Since the H-atom is also paramagnetic, it too can serve as an o/p catalyst within the solid. In addition, even at the low temperatures at which these experiments were conducted (1.93 K), the H-atom can still diffuse via quantum mechanical tunneling [10–15]. Thus, if the H-atom quantum diffusion rate is large, one H-atom can convert large numbers of oH_2 molecules over long distances. Under these conditions Eq. (5) for an immobile o/p catalyst would not be applicable, and instead for a mobile o/p catalyst X_o should decay exponentially until it reaches the equilibrium value $X_o \approx 0$ for the 2 K solid.

As shown in Fig. 9, X_o is observed to decrease exponentially from 0.02916 to 0.02358 within the ~500 min time interval. The solid line in Fig. 9 is the result of a least-squares fit of Eq. (3) to the X_o data and the fitted constants are reported in Table 4.

Table 4. Fitted parameters determined from least-squares fits of Eq. (3) to X_o data during IR exposure for two crystals with initial $X_o \approx 0.0295$ values

Crystal	$X_o(t = \infty)$	A	k, min^{-1}
c	0.02358(3)	$5.58(3) \cdot 10^{-3}$	$5.4(1) \cdot 10^{-3}$
d	0.02365(8)	$5.30(7) \cdot 10^{-3}$	$4.7(2) \cdot 10^{-3}$

Two separate experiments under the same experimental conditions (crystals c and d) show that the exponential decrease in X_o is very reproducible. However, X_o does not approach the 2 K equilibrium value ($X_o \approx 0$), but an infinite time value around $X_o(t = \infty) = = 0.02358$. We speculate that the reasons the H-atoms do not fully catalyze o/p conversion in solid hydrogen under these conditions are 1) preferential diffusion of the H-atoms in locally high pH_2 concentration regions of the crystal and 2) decay of the H-atom concentration with time. Based on ESR measurements, H-atoms tunnel through nH_2 solids leaving behind trails of pH_2 molecules, and subsequent H-atoms preferentially tunnel along these same pH_2 trails [12]. Preferential H-atom diffusion therefore can result in less o/p conversion in the solid than if the H-atom diffusion path were purely random. The H-atom concentration also decays in time primarily through H + H $\rightarrow$ H_2 recombination and under the present conditions the H-atom concentration has likely decayed to zero by the end of the 500 min IR exposure. The H-atoms are only produced while there are still Cl-atoms left to react. After the IR-induced reaction is over, then the H-atom concentration steadily decays. Fushitani and Momose [31] have studied H-atom recombination with NO in

solid pH_2 and observe H-atom decay via the growth of HNO on a similar timescale. Interestingly at very low $X_o = 0.001$ values the H-atom recombination rate slows down compared to the recombination rate at $X_o = 0.08$ [13]. It would therefore be worthwhile to repeat these studies of H-atom catalyzed o/p conversion for hydrogen solids with $X_o = 0.001$ instead of $X_o = 0.03$. We are currently designing new experiments to study H-atom catalyzed o/p conversion using FTIR spectroscopy over a greater range of conditions.

Quantitative measurements of the H-atom diffusion rate in solid hydrogen as a function of X_o are difficult to make, but the best models based on extensive ESR measurements indicate H-atom chemical diffusion speeds up at very low X_o values [13]. The rate of multidimensional H-atom tunneling in solid hydrogen is faster when the initial and final tunneling states are at the same energy, for example the H-atom position before and after the H-atom has moved one lattice spacing [12,13]. A very pure pH_2 crystal is homogeneous, periodic and symmetrical making this resonant H-atom chemical tunneling facile [12,13]. With the introduction of oH_2 impurities, resonant tunneling phenomena such as H-atom chemical diffusion slow down because the impurities detune the initial and final tunneling states. The H-atom diffusion rates might be inferred by modeling the o/p conversion kinetics measured in this work. We are interested in these quantum phenomena since H-atom tunneling in solid hydrogen is very similar to vibron hopping which is directly related to how the $Cl + H_2$ reaction is triggered by IR light [2,3,5].

4. Summary

The FTIR spectroscopic measurements presented here show that during the course of the IR-induced $Cl + H_2$ reaction in cryogenic solid hydrogen, qualitatively different o/p conversion mechanisms dominate depending on the initial X_o value for the crystal. At relatively high X_o values ($X_o = 0.5$), o/p conversion proceeds via oH_2 quantum diffusion to Cl-atom reaction centers. At these high X_o values, H-atom catalyzed conversion also likely occurs but at a negligible rate compared to the Cl-atom catalyzed o/p conversion. However, at low X_o values ($X_o = 0.03$) conversion proceeds almost exclusively via H-atom catalyzed o/p conversion. The rate of Cl-atom catalyzed conversion is small since the reaction rate is limited by oH_2 quantum diffusion to the Cl-atom reaction centers which slows down dramatically at low X_o values. In contrast, the H-atoms can still readily diffuse to the oH_2 molecules at low X_o values and thus H-atom catalyzed o/p conversion dominates.

Acknowledgments

1. T. Momose, M. Fushitani, and H. Hoshina, *Int. Rev. Phys. Chem.* **24**, 533 (2005).
2. K. Yoshioka, P.L. Raston, and D.T. Anderson, *Int. Rev. Phys. Chem.* **25**, 469 (2006).
3. P.L. Raston and D.T. Anderson, *Phys. Chem. Chem. Phys.* **8**, 3124 (2006).
4. P.L. Raston and D.T. Anderson, *J. Chem. Phys.* **126**, 021106 (2007).
5. S.C. Kettwich, P.L. Raston, and D.T. Anderson, *J. Phys. Chem.* **A113**, 7621 (2009).
6. M. Alagia, N. Balucani, L. Cartechini, P. Casavecchia, G.G. Volpi, F.J. Aoiz, L. Banares, T.C. Allison, S.L. Mielke, and D.G. Truhlar, *Phys. Chem. Chem. Phys.* **2**, 599 (2000).
7. G. Capecchi and H.-J. Werner, *Phys. Chem. Chem. Phys.* **6**, 4975 (2004).
8. X. Wang, *Science* **322**, 573 (2008).
9. L. Abouaf-Marguin and A.-M. Vasserot, *Chem. Phys. Lett.* **460**, 82 (2008).
10. V. Shevtsov, A. Frolov, I. Lukashevich, E. Ylinen, P. Malmi, and M. Punkkinen, *J. Low Temp. Phys.* **95**, 815 (1994).
11. T. Miyazaki, S. Mori, T. Nagasaka, J. Kumagai, Y. Aratono, and T. Kumada, *J. Phys. Chem.* **A104**, 9403 (2000).
12. T. Kumada, S. Mori, T. Nagasaka, J. Kumagai, and T. Miyazaki, *J. Low Temp. Phys.* **122**, 265 (2001).
13. T. Kumada, M. Sakakibara, T. Nagasaka, H. Fukuta, and J. Kumagai, *J. Chem. Phys.* **116**, 1109 (2002).
14. T. Kumada, *Phys. Rev.* **B68**, 052301 (2003).
15. T. Kumada, Y. Shimizu, T. Ushida, and J. Kumagai, *Radiat. Phys. Chem.* **77**, 1318 (2008).
16. S. Tam and M.E. Fajardo, *J. Chem. Phys.* **108**, 4237 (1998).
17. S. Tam and M.E. Fajardo, *Rev. Sci. Instrum.* **70**, 1926 (1999).
18. I.F. Silvera, *Rev. Mod. Phys.* **52**, 393 (1980).
19. M.E. Fajardo, *private communication*.
20. S. Tam, M.E. Fajardo, H. Katsuki, H. Hoshina, T. Wakabayashi, and T. Momose, *J. Chem. Phys.* **111**, 4191 (1999).
21. M. Pettersson and J. Nieminen, *Chem. Phys. Lett.* **283**, 1 (1998).
22. J. Eloranta, K. Vaskonen, H. Hakkanen, T. Kiljunen, and H. Kunttu, *J. Chem. Phys.* **109**, 7784 (1998).
23. S. Hubinger and J.B. Nee, *J. Photochem. Photobiol.* **A86**, 1 (1995).
24. A.C. Stanton, *Chem. Phys. Lett.* **122**, 385 (1985).
25. *Physics of Cryocrystals*, V.G. Manzhelii, Y.A. Freiman, M.L. Klein, and A.A. Maradudin (eds.), AIP Press, Woodbury, New York (1997).
26. J. Van Kranendonk, *Can. J. Phys.* **38**, 240 (1960).
27. H.P. Gush, W.F.J. Hare, E.J. Allin, and H.L. Welsh, *Can. J. Phys.* **38**, 176 (1960).
28. P.L. Raston and D.T. Anderson, *manuscript in preparation*.
29. B.J. Roffey, S.A. Boggs, and H.L. Welsh, *Can. J. Phys.* **52**, 2451 (1974).
30. V. Shevtsov, A. Scherbakov, P. Malmi, E. Ylinen, and M. Punkkinen, *J. Low Temp. Phys.* **104**, 211 (1996).
31. M. Fushitani and T. Momose, *Fiz. Nizk. Temp.* **29**, 985 (2003) [*Low Temp. Phys.* **29**, 740 (2003)].